Sudan University of Science and Technology

College of Graduate Studies

Wind Energy and Solar Energy Potential in the Red Sea Coast

إمكانية أستخدام طاقـة الرياح والطاقة الشمسية في ساحل البحر الأحمر

A thesis submitted in partial fulfillment of the requirement M.sc degree in physics

Prepared by :   **Supervised by :**

Tasabeeh Mohamed Alnasir Abd Alhakim   Prof . Mohamed Osman Sid- Ahmed

2016

الآيــــــــة

﴿ اللَّهُ نُورُ السَّمَاوَاتِ وَالأَرْضِ مَثَلُ نُورِهِ كَمِشْكَاةٍ فِيهَا مِصْبَاحٌ الْمِصْبَاحُ فِي زُجَاجَةٍ الزُّجَاجَةُ كَأَنَّهَا كَوْكَبٌ دُرِّيٌّ يُوقَدُ مِنْ شَجَرَةٍ مُبَارَكَةٍ زَيْتُونَةٍ لا شَرْقِيَّةٍ وَلا غَرْبِيَّةٍ يَكَادُ زَيْتُهَا يُضِيءُ وَلَوْ لَمْ تَمْسَسْهُ نَارٌ نُورٌ عَلَى نُورٍ يَهْدِي اللَّهُ لِنُورِهِ مَنْ يَشَاءُ وَيَضْرِبُ اللَّهُ الأَمْثَالَ لِلنَّاسِ وَاللَّهُ بِكُلِّ شَيْءٍ عَلِيمٌ ﴾

صدق الله العظيم

(سورة النور: الآية 35)

I

Dedication

All my progress and support comes from my family, without them I would never Have the courage to succeed in my studies and to achieve my life goals:-

All my dedication goes to,

My mother

     My father

          My professors

               My friends

                    To all My family members

               I thank you all

Acknowledgement

All thanks and gratefulness is for Allah, the most gracious, the most merciful.

First of all,I would like to thank Sudan University , my sincerity goes to my supervisor Prof. Mohamed Osman Sid- Ahmed for all the help and support he provided to me, always being there for me when I needed his help. Secondly, I would like to thank wind energy project UNDP for providing all the information I needed to help me complete my research.

Abstract

The Red Sea coast enjoys high values of wind speed and moderate values of solar radiation. Wind Atlas Analysis and Application Program (WAsP) has been used to analyze the wind data at Tokar, Free Zone and Port Sudan. The power densities at the three sites,at 50 m height,are 584, 288 and 300 W/m^2, respectively. Both solar and wind can be utilized to supply electricity to that area.

المستلخص

ساحل البحر الاحمر يتمتع بسرعات رياح عالية وإشعاع شمسي معتدل. تم تحليل سرعات الرياحفي طوكرو المنطقة الحرة وبورتسودان باستخدام برنامج (WAsP) . كثافات الطاقة على ارتفاع 50 م في المناطق الثلاثة 584و 288و 300واط \م^2 على التوالي.

Contents

Chapter one

Wind Basics

1.1 Introduction

Wind is clean, abundant, and a renewable energy resource that can be tapped to produce electricity. This chapter explores how wind is generated and introduces two types of wind, local and global. We'll also explore ways local topography affects wind, introducing two key concepts: ground drag and turbulence. This information provides the practical knowledge will need to select the best site for a wind turbine and the optimum tower height.

1.1 Offshore and onshore winds

Offshore and onshore winds are generated along the shores of large lakes. They are produced by the differential heating of land water, caused by solar energy, as shown in Fig 1.1a. When air is heated it expands, and as it expands it becomes less dense and rises. The upward movement of air is called a thermal or updraft.

Although water and land both heat up when warmed by the sun, land masses warm more rapidly than neighboring bodies of water.Because air over land heats up more quickly than air over water, air pressure over land is lower than over neighboring surface waters. As warm air rises over land, cooler, high pressure air moves in to fill the void, resulting in a steady breeze known as onshore wind. At night, the winds blow in the opposite direction from land to water as illustrated in Fig 1.1b. These are known as offshore breezes or offshore wind.
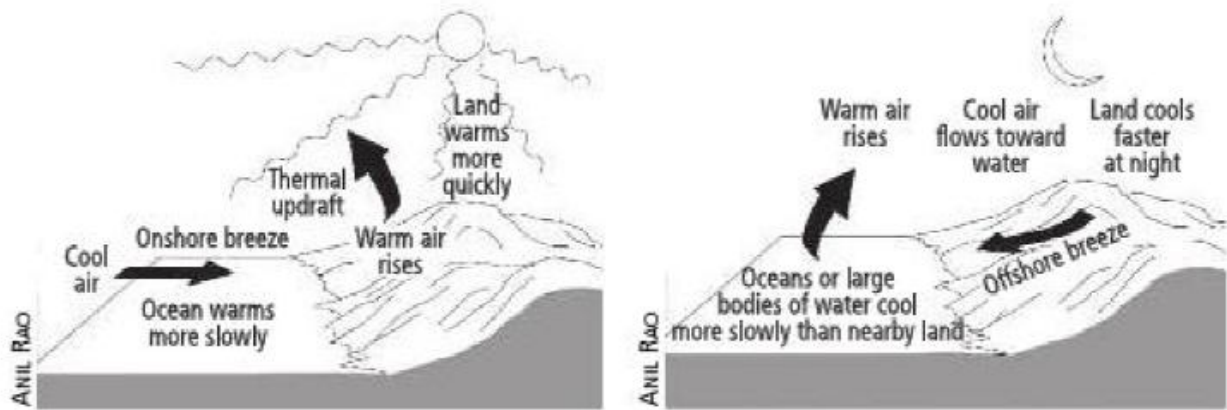
Fig 1.1a and 1.1b: Onshore and offshore breezes. Onshore (a) and offshore (b) breezes occur along the coastlines of major lakes and oceans [1].

Like onshore winds that occur during the day, offshore winds are created by differences in air pressure between the air over land and neighboring water bodies. After sunset, the land and the ocean both begin to cool. Land, however, cools more rapidly than water. Because the water cools more slowly, air above it is warmer. Warm air expands and rises. Cooler high pressure air Flows from the land to the water at night Fig1.1b. The result is an offshore breeze: steady winds that flow from land to water. Offshore and onshore breezes operate day in and day out on sunny days, providing a steady supply of wind energy. Because offshore and onshore winds are fairly reliable, coastal regions of world are often ideal locations for small (and large) wind turbines. Coastal winds are more consistent than winds over the interior of continents and also tend to be more powerful because of the relatively smooth and unobstructed surface of open waters. That is to say wind moves rapidly over water because lakes and coastal waters provide very little resistance to its flow, unlike forests or cities and suburbs, which dramatically lower surface wind speeds.

1.2 Mountain-Valley Breezes

Like coastal winds, mountain-valley breezes arise from the differential heating of the Earth's surface. In the morning on the clear days the sunrays strike the valley floor and begin heating the ground, valley walls and mountains. As the ground and valley walls begin to warm, the air above them warms.It then expands and begins

2

to flow upward. This process is known as convection. While some of this warm air rises vertically, mountain valleys also tend to channel the solar-heated air through the valley toward the mountains, Fig 1.2. Winds flow in reverse at night because the mountains cool more quickly than the valley floor. Cool, dense air (high-pressure air) from the mountains sinks and flows down through the valleys like the water in a mountain stream creating steady and often predictable down – valley or mountain breezes. Together, valley and mountain winds are known as mountain-valley breezes. Mountain-valley breezes typically occur in the summer, a time when solar radiation is greatest and also typically occur on calm days when the prevailing winds are weak or nonexistent.
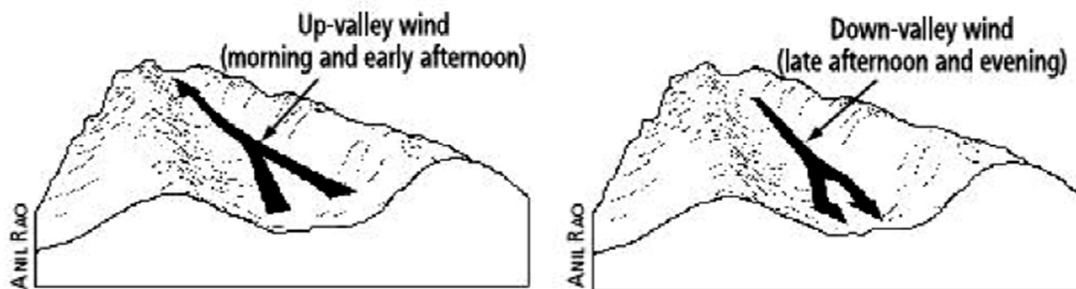
Fig 1.2a and 2.2b: mountain – valley breezes. Mountain – valley winds can provide a reliable source of wind power if conditions are just right.

(a) up- valley winds. (b) down- valley winds [1].

Mountain-valley winds also form in the presence of prevailing winds- for example, when a storm moves through an area. In such instances, mountain or valley winds may "piggy back " on the prevailing winds, creating even more powerful (and hence higher energy) winds. When consistently flowing in the same direction, such winds can provide a great deal of power that can be tapped to produce an abundance of electricity.

1.3 Large-Scale wind Currents

Local winds can be a valuable source of energy. The winds on which most people rely, however, are those produced by much larger air masses that result from regional and global air circulation. They create dominant wind-flow patterns,

known as prevailing winds.Prevailing winds, like local winds, are created by the differential heating of the Earth's surface, but on a much larger scale. They are formed: As shown in Fig 1.3, the Earth is divided into three climatic zones: the tropics, temperate zones and poles.
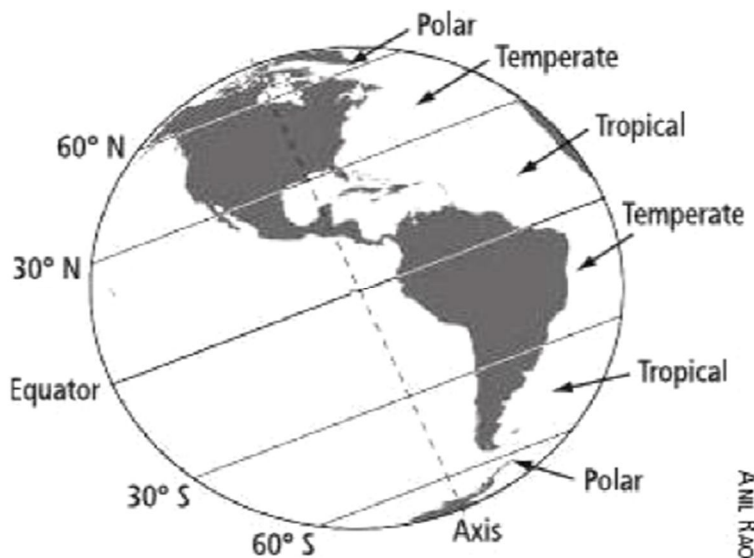
Fig 1.3: climate zones. The Earth divided into three climate zones in each hemisphere. In the northern hemisphere, warm air from the tropics flows northward by convection, creating the global circulation pattern [1].

Because the tropics are more directly aligned with the sun throughout the year, they receive more sunlight and are, therefore, the warmest regions on Earth. The temperature zones lie outside the tropics, in both the northern and southern hemispheres. They receive less sunlight than the tropics and so are cooler. The north and south poles receive the least amount of sunlight and are the coolest regions of our planet. As shown in Fig1.4a, global air circulation is created by hot air produced in thetropics. This air expands and rises (as in local air circulation patterns). Cool air from the northern regions as far north as the poles moves in to fill the void. The result is huge air currents that flow from the poles to the equator. Although air generally flows from the north and south poles toward the equator, circulation patterns are a bit more complicated. In northern hemisphere, some of the warm air moving northward cools and sinks back to the earth's surface, as shown in Fig 1.4b. It then flows back toward the equator creating the trade winds.

Because the trade winds blow quite consistently, they are a potentially huge and reliable source of energy for residents and nations fortunate enough to lie in the wind's path. As shown in Fig 1.4b, a substantial amount of the northward – moving air continues on toward the North Pole, travelling over the temperature zone. The Fig also shows air masses flowing northward across the temperature zone split into two, creating higher - and lower –level winds. When the upper winds reach the North Pole, this cold air sinks and then flows southward back toward equator. If no other forces were at work, winds flowing back to equator would flow from north to south. As shown in Fig 1.4c, they don't. Other factors influence the movement of air masses across the surface of the planet. One of the most significant is the Earth's rotation, which results in a phenomenon known as the Coriolis Effect.
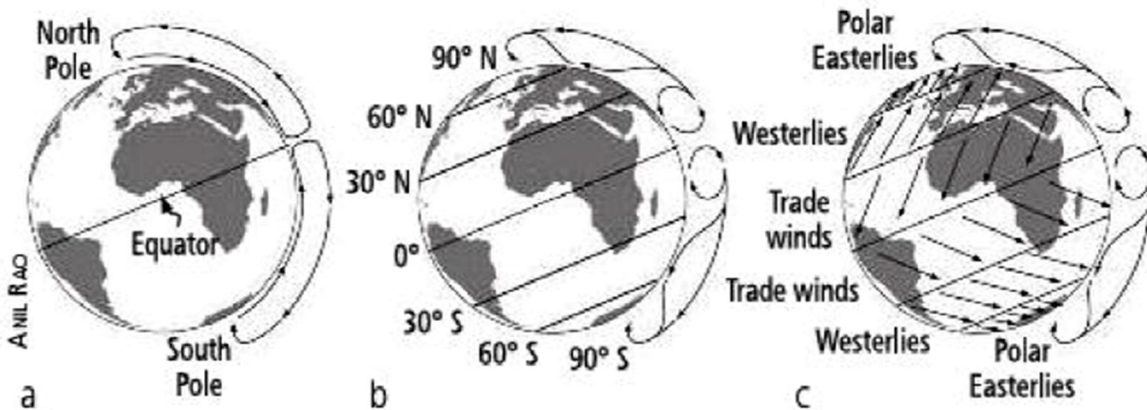
Fig: 1.4: global air circulation. (a) As shown here, warm tropical air rises and flows toward the poles. Cold polar air flows toward the equator. (b) Warm tropical air loses some of its heat and sinks toward the earth's surfaces, then flows back towards] the equator, creating the trade winds. Air masses moving over temperate zone split into upper and lower wind. (c) Wind patterns caused by the Coriolis Effect, resulting from the rotation of the earth on its axis [1].

1.4 The Coriolis Effect

As shown in Fig1.4c, the trade winds in northern hemisphere flow from northeast to southwest. As shown in Fig 1.5, as the plane travels south, the earth rotates beneath it. The earth rotates eastward. The plane appears to have been deflected. In

reality, it only looks that way. The apparent deflection of the plane's path is the Coriolis effect. In the northern hemisphere, the deflection is to the right of the direction of travel. In the southern hemisphere, the deflection is to the left. Winds flowing north or south also appear to be deflected. The south – flowing trade winds, for instance, appear to flow from northeast to southwest. In the temperature zone, as shown in Fig 1.4c, the low- level north – flowing winds that sweep across the surface of the earth flow across the north American continent not from south to north but from southwest to northeast. These are the prevailing southwesterly winds that blow across the Great Plain of north America. Many wind farms and many a small wind operation depending on them.
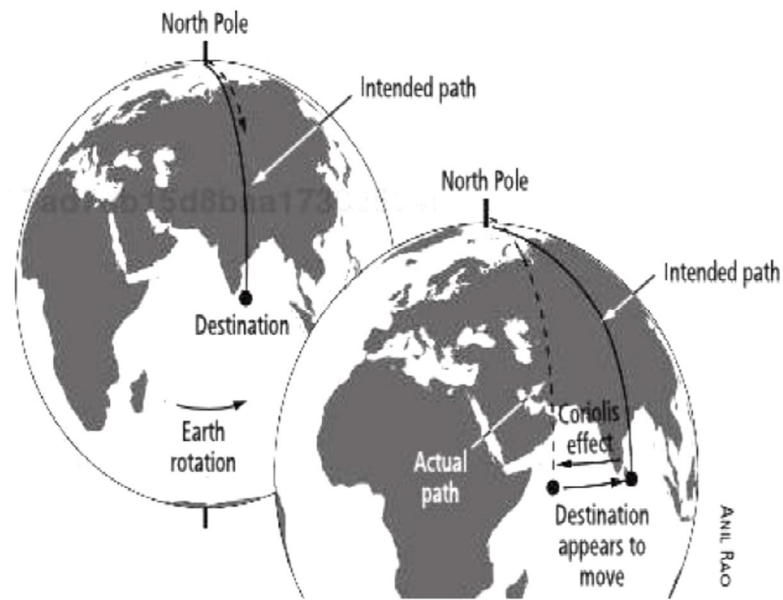
Fig 1.5: the Coriolis Effect [1].

1.5 Wind from storms

Storms, in turn are produced when high-pressure and low-pressure air masses collide. High and low pressure zones move across the continents.Low-pressure air masses originate in the tropics. They are created by the huge influx of solar energy in these regions. Huge masses of low-pressure air frequently break away and migrate northward, sweeping across the North American continent. High-pressure air masses originate in the north and south poles, regions of more or less permanent cold, high-pressure air. Like warm tropical air, huge masses of cold arctic air also

6

break loose and drift southward, sweeping across the northern hemisphere. The greater the difference in pressure between a high-pressure air mass and a "neighboring" low-pressure air mass, the stronger the winds. In some cases, these winds contain an enormous amount of energy.

1.6 Friction and Turbulence

Wind does not flow smoothly over the Earth's surface. It encounters resistance, known as friction. This results in a phenomenon called ground drag. Ground drag is caused by friction when air flows across a surface. Ground drag due to friction, however, varies considerably, depending on the roughness of the surface. The rougher or more irregular the surface, the greater friction. As a result, air flowing across the surface of lake generates less friction than air flowing over a meadow. Air flowing over a meadow generates less friction than air flowing over a forest. Friction extends to a height of about 1500 meters. However, the greatest effects are closest to Earth's surface, Fig .1.6 .
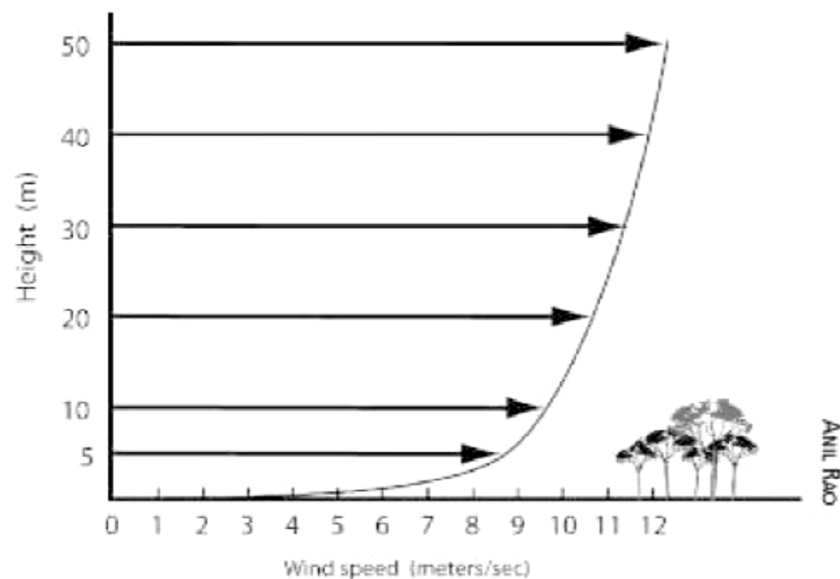
Fig 1.6: Effect of Ground Drag [1].

Another natural phenomenon that affects the output of most wind turbines is turbulence. Turbulence is produced as air flowing across the Earth's surface encounters objects, such as trees or buildings. They interrupt the wind's smooth laminar flow, causing it to tumble and swirl, the same way rocks in a stream interrupt the flow of water. Rapid changes in wind speed occur behind large

7

obstacles and winds may even flow in the direction opposite to the wind. This highly disorganized wind flow is referred to as turbulence.Proper location is the key to avoiding the damaging effects of turbulence. Turbulence can also be minimized by mounting a wind turbine on a tall tower. In sum, then, mounting a wind generator on a tall tower offers four benefits: (1) it situates the wind generator in the stronger higher-energy-yielding winds, substantially increasing electrical production, (2) it raises the machine out of damaging turbulent winds, (3) it decreases the wind turbine's maintenance and repair requirements, and (4) it increases the wind turbine's useful lifespan substantially, perhaps tenfold [1].

1.7 Objectives

The objective of this work is to study the wind and solar energy resources at the Red Sea coast and the expected power density from these resources.

Chapter 2

Wind and Wind Conversion

2.1 Wind energy in Sudan

Fig.2.1 Annual mean wind speed at 80m height.

Sudan is blessed with significant wind energy resource. The annual mean wind speed is between 8.1 and 4.5 m/s at height 80 m [2].
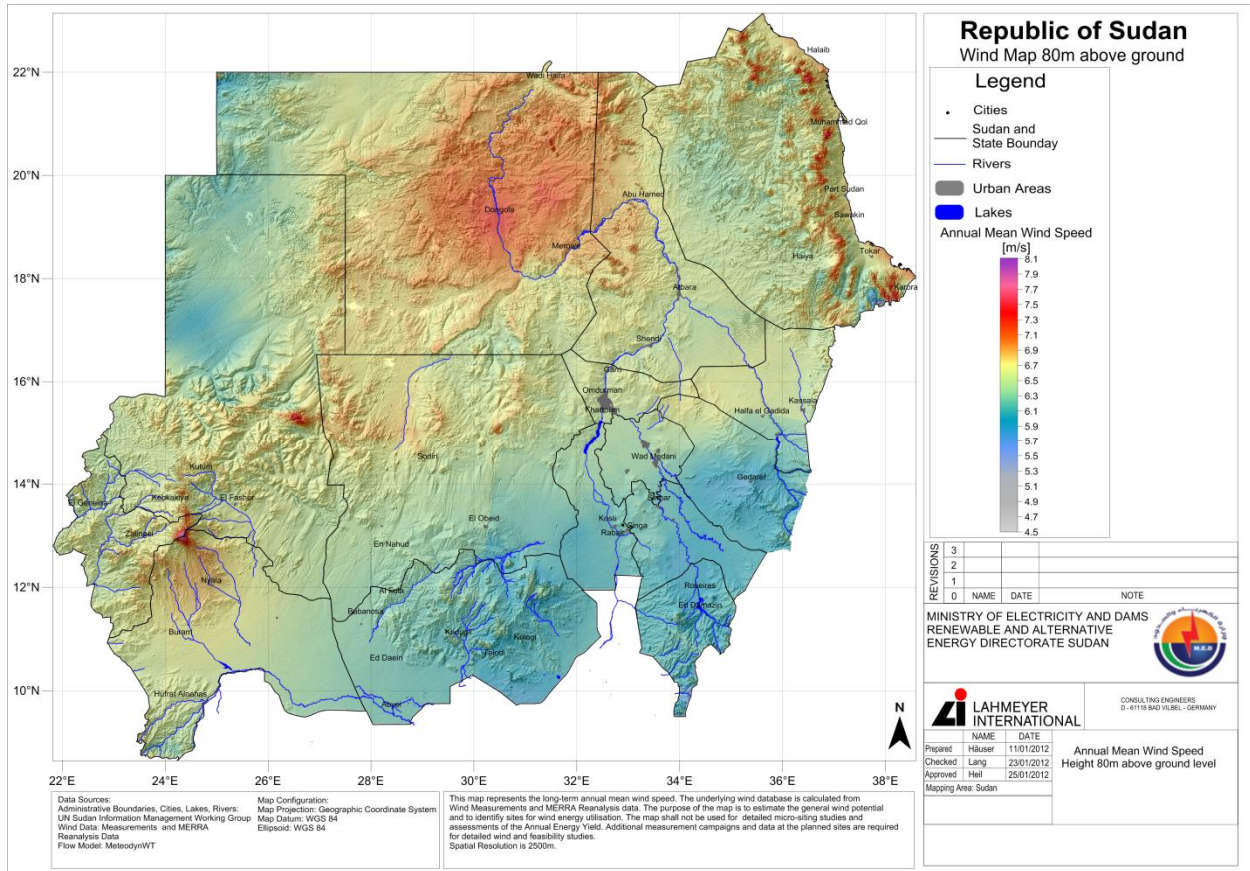
2.2 The mathematics of wind power

To understand how important is to mount a wind turbine on a tall tower, consider a simple mathematical equation. It's called the power equation and is used to

calculate the power available from the wind. This equation shows that three factors influence the output of a wind energy system: (1) air density, (2) swept area, and (3) wind speed. The power equation is

$$P = \frac{1}{2}\rho A \, v^3. \tag{1.1}$$

P stands for the power available in the wind (not the power a wind generator will extract that's influenced by efficiency and other factors). Density of the air is ρ. Swept area is A. Wind speed is V.

2.2.1 Air density

Air density is the weight of air per unit volume, which varies with elevation. As a general rule, anticipate a decrease in the air density of about 3 percent per 300 meters increase in elevation [1].As a result, air density doesn't affect the power available from the wind until elevation reaches 760 meters above sea level.

2.2.2 Swept Area

Swept area is the area of the circle that the blades of a wind machine create when spinning. It is a wind machine's collector surface. The larger the swept area, the more energy a wind turbine can capture from the wind. Swept area is determined by blade length. The longer blades, the greater swept area. The greater swept area, the greater electrical output of a turbine. As the equation suggests, the relationship between swept area and power output is linear. Theoretically, a ten percent [1] increase in swept area will result in a ten percent increase in electrical production. Doubling the swept area doubles the output. Swept area can be calculated using the equation $A = \pi r^2$. In this equation, A is the area of the circle, the swept area of the wind turbine. For a wind turbine, radius is usually about the same as the length of the blade.
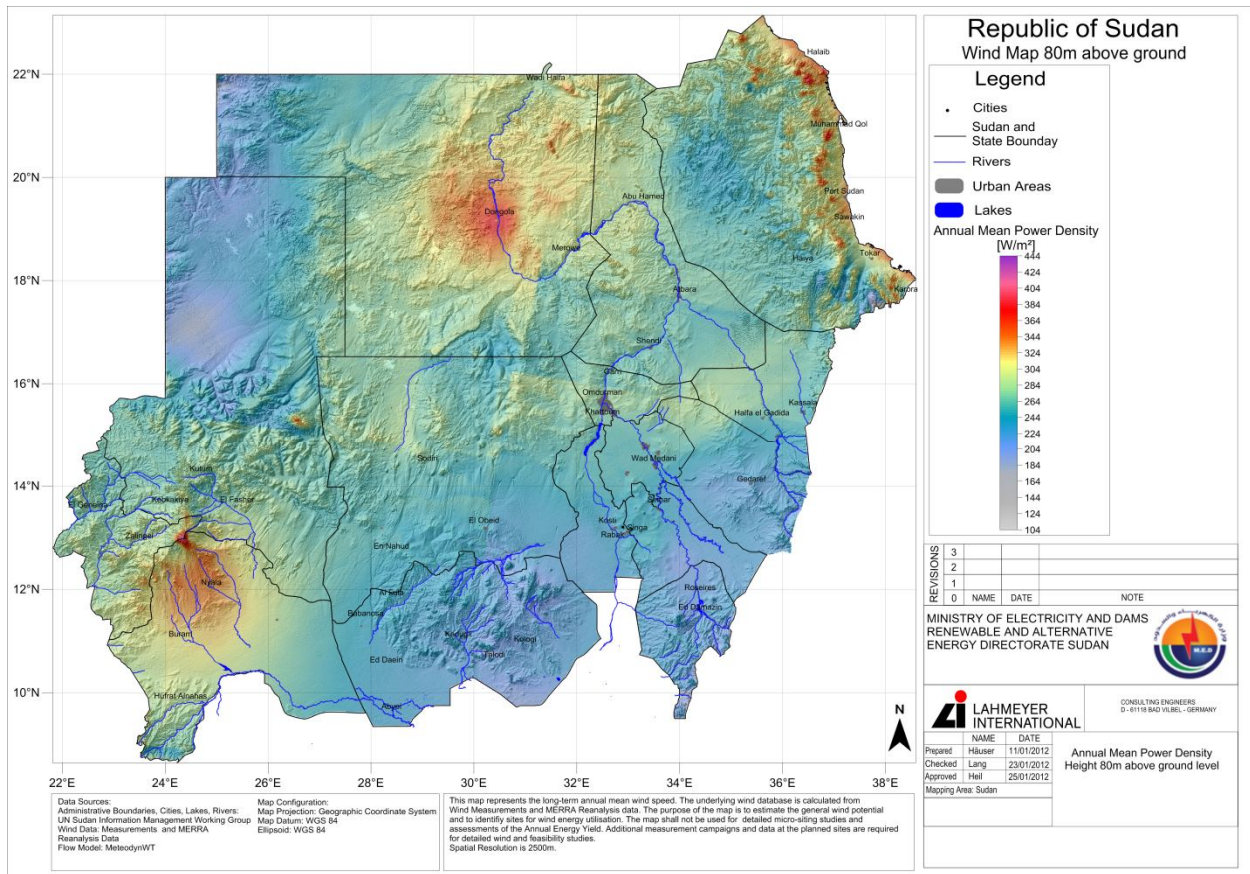
Fig.2.2 Annual mean power density in Sudan at height 80m.

The annual mean power density is between 444-104 W/m^2 at height 80m. The maximum power density is at north-east of Sudan. The power density at the Red Sea coast is about 340 W/m^2 [2]. This is about 8 kWh m^{-2}/day.

2.3 Wind turbine design

The design and size of a turbine paly crucial role in electricity generation .Maximum wind capture and cost reductions are two primary motives of wind turbine research. Continuous research and advancement of turbine technology have taken place over the last several decades. As a result, nameplate capacity rating has risen enormously. Today, commercially available wind turbines have rating ranging from kilowatt to megawatts .The diameter of the turbine is an important parameter .The recent trend is toward large turbines ,as longer blades sweep wind from a larger area and produce greater output energy.Modern wind turbines can be

divided into two types: (1) horizontal axis wind turbines (HAWTs) and (2) vertical axis wind turbines (VAWTs). HAWTs dominate the majority of the wind industry due to their greater efficiency and energy output in comparison to VAWTs. VAWTs are inherently problematic in that they are installed close to the ground and therefore have less exposure to wind, which in turn leads to less power output. In order to achieve the same output as that of HAWTs, VAWTs require more material and greater size, which in turn result in a significantly greater cost. However, VAWTs still can produce at least some electricity in low winds and have low noise level can capture wind from any direction. VAWTs have been proven to be effective in rooftop and small scale applications. When air flows over any surface, it creates two types of aerodynamic forces: one in direction of the airflow (known as drag force) and another perpendicular to the airflow (known as lift forces). One or more of these forces can be used to generate the driving torque needed to rotate the blades. Modern wind turbines work on aerodynamic lift forces. A wind turbine typically consists of blades, a rotor, a tower, a gearbox and generator.

A rotor consists of large blades resembling an airplane wing. Three blades for universally accepted, but two blade turbines are also functional. Rotor blades are very large in size. Another component called the "pitch drive "is used to reduce the effect of lift forces in high wind speed conditions.Nacelle-nacelle is located at the top of the turbine tower. It is attached to the rotor, and contains the main technical parts, such as the rotor shaft, gearbox and generator. The nacelle is connected to the tower with bearings and is able to rotate with respect to the wind direction in order to harness maximum wind energy.The generator converts the mechanical energy of the rotor into electrical energy.Tower and foundation- speed, quality (less turbulence and turmoil), and quantity of wind increase with the increment of height. A tower is used to place the rotor at high altitudes in order to capture more wind energy.

Additionally, a controller, anemometer, heat exchanger and wind vane are other important components in a wind turbine. The controller is a computer operated system that controls the turbine's operation, the heat exchanger cools the generator, the anemometer measures wind speed, and the wind vane detects wind direction [3].

2.4 Onshore wind turbines

On shore wind turbines, a category that is installed on land, has 50-100meters tower height with a rotor diameter of 50-100m. The general trend in wind turbine designs is to increase tower height and rotor blade length. A combination of high pole and long blades allow wind turbines to be installed in areas with low wind energy potential.Modern turbines work on a rotor and hub assembly speed of 12-20 RPM [3]. As result, modern turbines are capable of effectively generating power at much lower wind speeds. Additionally, these turbines have a significantly higher electricity generation capacity. In present day, storm controlled techniques enable wind turbines to operate even during very high wind speed conditions. On shore wind turbines are typically grouped together into wind power plants, commonly known as wind project or wind farms. These wind power plants are usually 5-300MW [3] in size, although smaller and larger plants are also in operation.

2.5 Offshore wind turbines

Wind turbines installed beyond the coast are known as offshore power systems. Offshore wind flows with higher speed and more uniformity than on land. Offshore sites have the ability to establish larger power plants with larger wind turbines. Offshore wind turbines usually have more nameplate capacity rating than onshore ones. Addressing issues such as lack of available land, less wind resources and social and environmental issues associated with onshore wind power projects have drawn great interest and investment in offshore power projects worldwide [3]. To measure the potential of wind power production at a specific location, we develop a quantitative and objective wind energy index represents the actual wind energy production of certain turbine type. To obtain such an index, there are several necessary steps. First, the type of database to calculate the wind energy index has to be chosen. A possible database is energy production data from wind farm in the neighborhood with similar wind conditions and turbine characteristics.

Alternatively, wind speed data can be applied directly. If wind speed data are chosen for the database, they have to be transferred to the wind turbine position since they are usually not available for every location. This means that the data have to be horizontally interpolated to the turbine location and vertically

extrapolated to the turbine height. The most crucial decision is how local wind speed data can be transformed to wind energy index that reflects actual wind energy production. Another way of analyzing the energy potential is to drive a wind energy index based on wind speed data, which are more readily available than production data. The most common dataset used in the analysis of wind resource is weather station data because it objectively measures the actual wind speed at certain locations. Using weather station data for this aim, however, comes under criticism: the availability of such data is often limited; the historical data records might be not complete; weather stations may not be located at a reasonable distance to wind farms [4].

An alternative dataset that has been recommended in the wind power analysis is reanalysis data, such as the Modern-Era Retrospective analysis for research and applications (MERRA) data provided by NASA. MERRA reanalysis

data reconstruct the atmospheric state by integrating data from different sources, such as conventional and satellite data. The wind data consist of a northward and an eastward wind component at three different height(2 m, 10 m, 50 m above the ground), which are helpful to drive the wind speed and wind direction at various turbine heights [4].

2.6 Horizontal interpolation

Every location lies within rectangle spanned by the four nearest MERRA grid points. The wind speeds at these four points i.e. the eastward northward components u_h and v_h at heights of 2m, 10m and 50m, are interpolated to the turbine's location weighted by their horizontal distance (inverse distance weighting). This approach assumes that the influence decreases with increasing distance. Given the rather short distances (maximum distance to the nearest grid point is about 35 kilometers) and the regular pattern of the MERRA grid, inverse distance waiting is a reasonable candidate. Nevertheless, alternative interpolation methods such as polynomial, or spline interpolation are possible.

After interpolating, the two components for each height are combined to obtain absolute value of the wind speed the turbine location the three heights using the Pythagorean Theorem:

$$V_h = \sqrt{u_h^2 + v_h^2}, \, h = 2, \, 10, \, 50. \hspace{3cm} (2.2)$$

At this point it is still possible to calculate the wind direction at height h, ϕ, at the turbines location with the following equation:

$$\phi = \tan^{-1}\left(\frac{v_h}{u_h}\right) \hspace{3cm} (2.3)$$

Because most wind turbines can rotate towards the wind direction, we neglect the wind direction in the following analysis and focus only on the wind speed.

2.7 Vertical extrapolation

The hub height of a typical wind turbine is much higher than 2m, 10m and 50m, where wind speeds are proved by MERRA. Hence, the valuable wind speeds at height h need to be extrapolated to the turbine height z. One extrapolation method is given by the power law

$$V_z = V_h\left(\frac{z}{h}\right)^\alpha \hspace{3cm} (2.4)$$

Where V_z and V_h denote the wind speeds at heights z and h, respectively. The wind shear coefficient α depends on the stability of the atmosphere can be derived empirically, but the results are very sensitive to correct modeling and assumptions. The power law gives a "reasonable first approximation" .However this procedure commonly used in the literature applied in this study is log wind profile

$$V_z = \left(\frac{U_*}{K}\right)\log\left[\left(\frac{z-d}{z_0}\right)\right] \hspace{3cm} (2.5)$$

Where V_z denotes the wind speed at height z, u_*, the friction velocity, the von karmanconstant($\sim$0.41) used for fluid modeling , d the displacement height , and z_0 the surface roughness. The three unknown parameter u, d, and z, can be calculated by solving the three dimensional equation system for the wind speeds at 2 m, 10 m and 50 m. By plugging in the turbine height for z, the desired wind speed at turbine height z, V_z, can be obtained [4].

2.8 conversion of wind speed to production

When the wind speed at the turbine position is derived, the most crucial step is the conversion into produced energy. One method is to apply a physical transformation, such as the wind power density (WPD), which describes how much kinetic energy from the wind per area can be transformed into energy production. The efficiency of the turbine can be included in Eq. (1.1), then the power density can be written as

$$\text{WPD} = \frac{1}{2}\rho C_p V_z^{3} \tag{2.6}$$

Where V_z denotes the wind speed at turbine height z, ρ the air density, and C_p the Betz limit (=16/27), which describes the maximum amount of energy a turbine can theoretically extract from the wind. The unit of WPD is w/m^2. By multiplying the WPD with the circular area spanned by the rotor blades (=diameter x π). Empirical evidence shows, however, that WPD overestimates the real on-site production and should be used only as an illustrative point [4].

Chapter 3
Solar Energy

3.1 Solar radiation in Sudan

Sudan has large solar energy potential. Solar energy, averaging 6.1kWh m^{-2}/day [5], is particularly significant, and is considered one of the best solar resources globally. As shown in Fig 3.1, the maximum is about 7 kWh m^{-2}/day in the north- western of the country. The minimum is about 5 kWh m^{-2}/day, at the Red Sea coast. Since solar radiation is available locally, this facilitates the provision of energy services to rural settlements that are unlikely to be reached by modern energy infrastructure (electric grid and pipelines) in the foreseeable future.

Recently, solar energy applications have become more popular, because of the decrease in cost and the increase in the efficiency of solar cells. In the following sections we review the theory of solar cells and the recent development in the technology of solar cells.
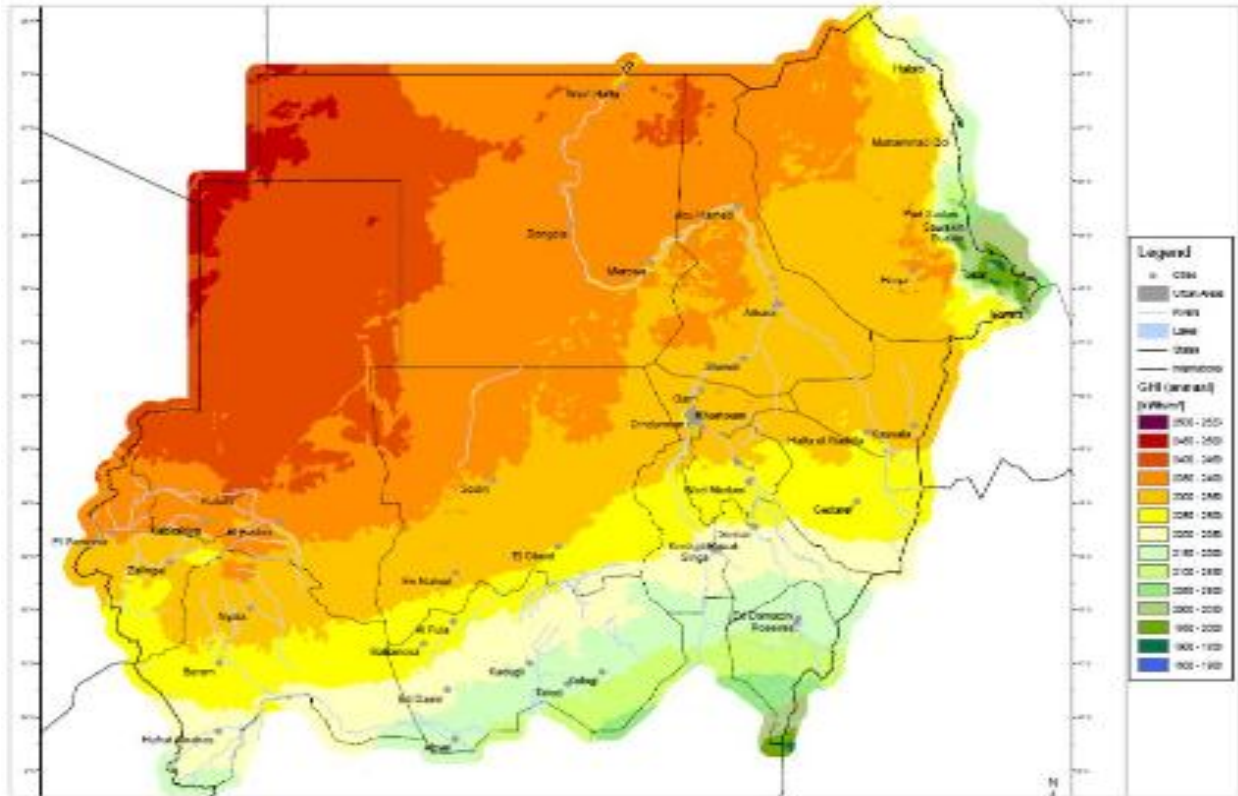
Fig.2.3 solar radiation in sudan[2].

3.2 Theory of Solar Cells
3.2.1 p-n Junctions

p-n junctions consist of two semiconductor regions of opposite type. Such junctions show a pronounced rectifying behavior. They are also called p-n diodes. The p-n junction is a versatile element, which can be used as a rectifier, as an isolation structure and as a voltage-dependent capacitor. In addition, they can be used as solar cells, photodiodes, light emitting diodes and even laser diodes. They are also an essential part of Metal-Oxide-Silicon Field-Effects-Transistors (MOSFETs) and Bipolar Junction Transistors (BJTs).

The left side in Fig.2.1 is the p-type with an acceptor density Na, while the region on the right is n-type with donor density N_d. The do pants are assumed to be shallow, so that the electron (hole) density in the n-type (p-type) region is approximately equal to the donor (acceptor) density [6].

18

Fig 3.2 Cross-section of a p-n junction [5]

3.3 solar cells

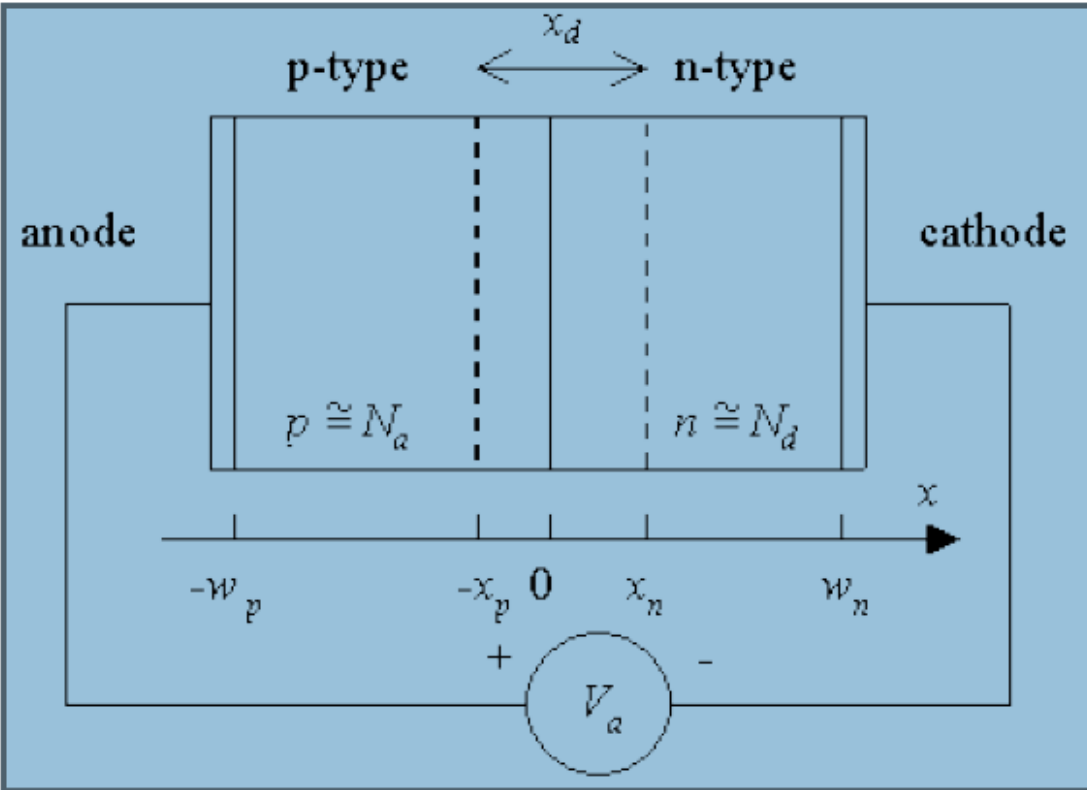Solar cells are typically illuminated with sunlight and are intended to convert the solar energy into electrical energy. The solar energy is in the form of electromagnetic radiation, The sun's spectrum is consistent with that of a black body at a temperature of 5800 K. The radiation spectrum has a peak at 0.8 eV. A significant part of the spectrum is in the visible range of the spectrum (400 - 700nm).

Only part of the solar spectrum actually makes it to the earth's surface. Scattering and absorption in the earth's atmosphere, and the incident angle affect the incident power density. Therefore, the available power density depends on the time of the day, the season and the latitude of a specific location. Of the solar light, which does reach a solar cell, only photons with energy larger than the energy band gap of the semiconductor generate electron-hole pairs. In addition, one finds that the voltage across the solar cell at the point where it delivers its maximum power is less than the band gap energy in electron volt.

The overall power-conversion efficiency of single-crystalline solar cells rangesfrom 10 to 30 % yielding 10 to 30 mW/cm^2 [6]. the cell to be positive as it

leads to electrical power generation. The power generated depends on the solar cell itself and the load connected to it
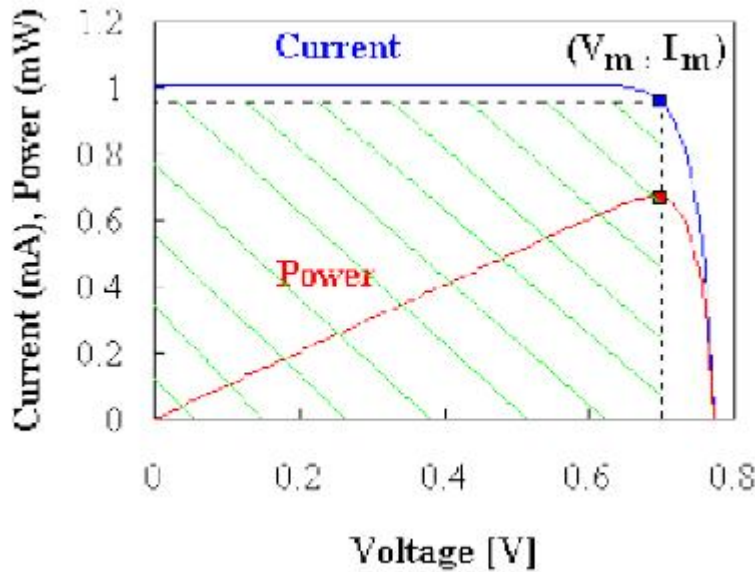
Fig 3.3 Current-Voltage (*I*- and Power-Voltage (*P-V*) characteristics of a p-n diode solar cell with $I_{ph} = 1$ mA and $I_s = 10^{-10}$ A. The crosshatched area indicates the power generated by the solar cell [5].

The open-circuit voltage, V_{oc}, is the voltage across the illuminated cell at zero current, Fig 3.3. The short-circuit current, I_{sc}, is the current through the illuminated cell if the voltage across the cell is zero. The short-circuit current is close to the photocurrent while the open-circuit voltage is close to the turn-on voltage of the diode as measured on a current scale similar to that of the photocurrent. The power equals the product of the diode voltage and current and at first increases linearly with the diode voltage but then rapidly goes to zero around the turn-on voltage of the diode. The maximum power is obtained at a voltage labeled as V_m with I_m being the current at that voltage.

The fill factor of the solar cell is defined as the ratio of the maximum power of the cell to the product of the open-circuit voltage, V_{oc}, and the short-circuit current, Isc, or:

$$\text{Fill Factor} = \frac{I_m V_m}{I_{sc} V_{oc}} \qquad\qquad (3.1)$$

3.4 Most common types of solar cells
3.4.1 Nano-pillar solar cell
The main requirement for any competitive photovoltaic (PV) technology is the cost per watt installed. To achieve this goal, a PV technology must not only have a low unit area cost, but also high efficiency. Nano-pillar (NPL) and nanowire (NW) PV address these requirements [6]:

(1) direct growth of crystalline materials on low-cost substrates without the use of complex epitaxial processes.

 (2) maximization of carrier collection efficiency by decoupling the light absorption and carrier collection directions.

(3) minimization of optical losses by reduced reflection and enhanced absorption.

Significant work has been carried out in recent years on all aspects of NPL/NW photovoltaics including synthesis, optical properties, and device physics. Of the possible architectures for NPL PVs, the two that enable enhanced carrier collection are NPLs embedded in a film, Fig 3.4(a), and core-shell NPLs, Fig 3.4(b). Considering these architectures, the optical and electronic design constraints on NPL PV are considerably relaxed compared to their planar counterparts. To prevent efficiency degradation through optical losses, the thickness of the cell must be greater than the absorption length of the material, Fig 3.4(c). Due to the excellent antireflective and light trapping properties of wire arrays, a significantly lower volume of active material, as compared to planar cells, can be used to absorb the majority of the incident solar photons. Similarly, by carefully tuning the geometry of the NPL cell, it is possible to maximize minority carrier collection for a given material quality. This design parameter is not available to planar cells since the carrier collection and light absorption directions are parallel. This design parameter enables NPL PV from even moderate quality materials to display excellent carrier collection efficiencies. However, the surface and interface area in NPL PV is significantly enhanced over planar cells [6].
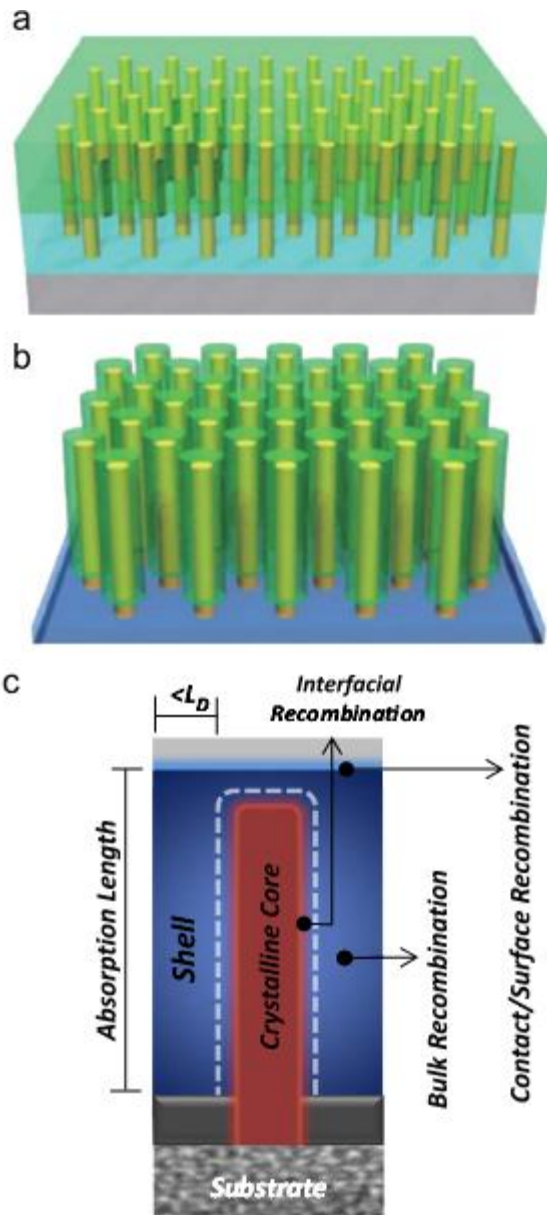
Fig 3.4 Nano-pillar architectures. (a) Array of NPLs embedded in a thin film; (b) NPL radial junctions; (c) schematic of a NPL PVcell with important lengths and recombination processes identified[6].

In a planar cell, carriers are collected along the same axis that light is absorbed Fig 3.5 a, requiring the diffusion length of carriers to be on the order of the absorption length of the material of choice. Since absorption lengths are on the order of microns, efficient planar PV requires high-quality, and often costly materials. On the other hand, minority carrier collection efficiency in NPL PV Fig 3.5 b is independent of the length, and only a function of NPL pitch.

 Fig 3.5 Carrier collection advantages of NPL solar cells. Schematics illustrating charge separation in (a) thin-film solar cells and (b) NPL solar cells. Simulation structure used to generate (d) short circuit current as a function of NPL center to center pitch for a fixed NPL diameter for two different minority carrier diffusion lengths [6].

3.4.2 Organic solar cells employing electrodeposited nickel oxide nanostructures

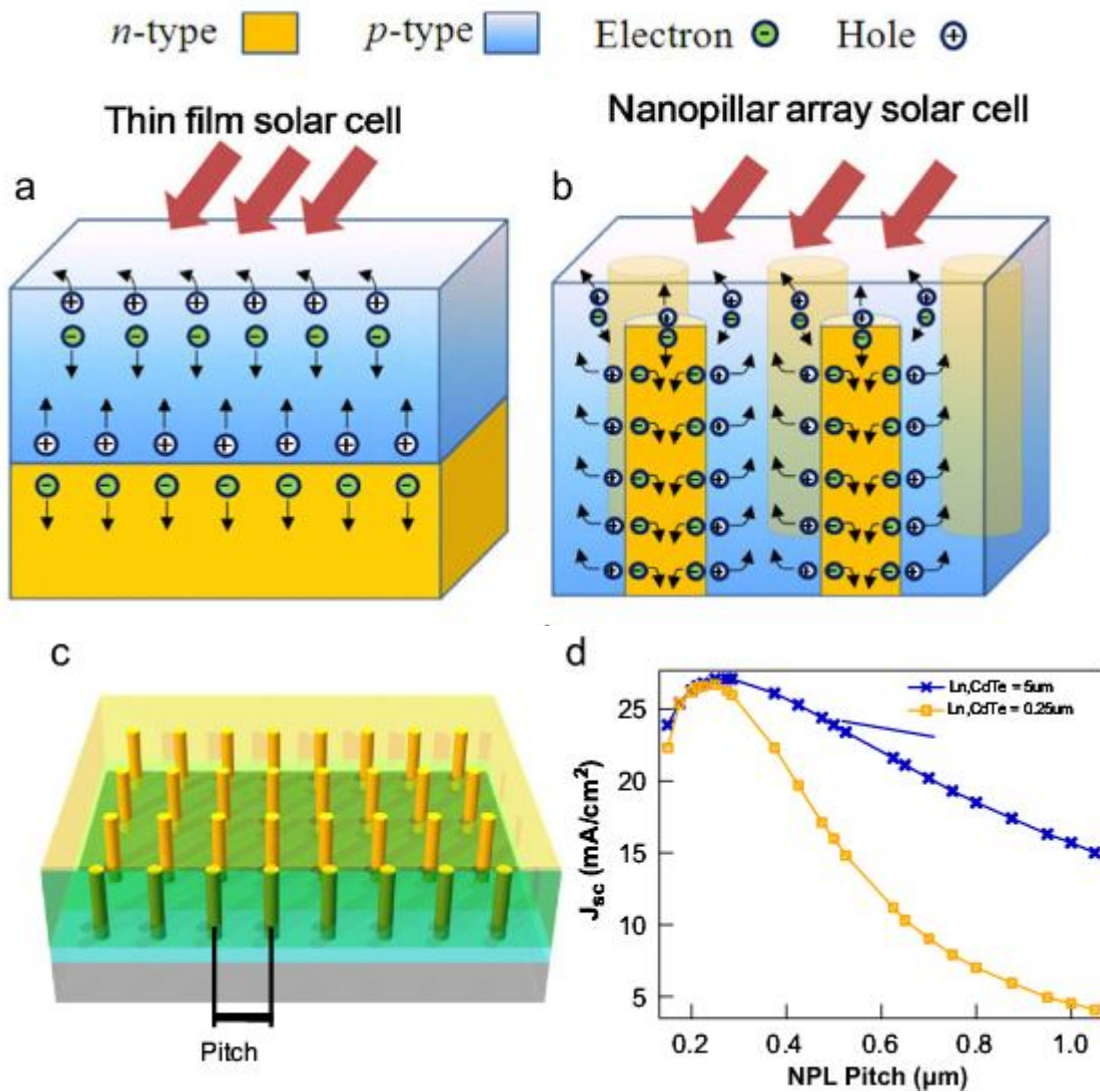An electrodeposited nickel oxide (NiO) nanostructure was used as an anode buffer layer in organic photovoltaic cells. The structure of NiO films were tailored by current density and electrodeposition time to have interconnecting nano-rods on indium tin oxide surface. When $-CF_3$-modified NiO structures were used as hole transporting and electron blocking layers. The bestpower conversion efficiency (3.05%) was achieved under an illumination of AM 1.5G (100 mW/cm^2) for a device with the interconnecting nano-rods NiO buffer layer [7].

3.4.3 The dye-sensitized solar cell

Dye-sensitized solar cell (DSSC) is a semiconductor photovoltaic device that directly converts solar radiation into electric current. The system consists of the following, Fig 3.6 [8]:

(1)   A transparent anode made up of a glass sheet treated with a transparent conductive oxide layer.
(2)   A mesoporous oxide layer (typically, TiO$_2$) deposited on the anode to activate electronic conduction.
(3)   A monolayer charge transfer dye covalently bonded to the surface of the mesoporous oxide layer to enhance light absorption.
(4)   An electrolyte containing redox mediator in an organic solvent effecting dye-regenerating
(5)   A cathode made of a glass sheet coated with a catalyst (typically, platinum) to facilitate electron collection.
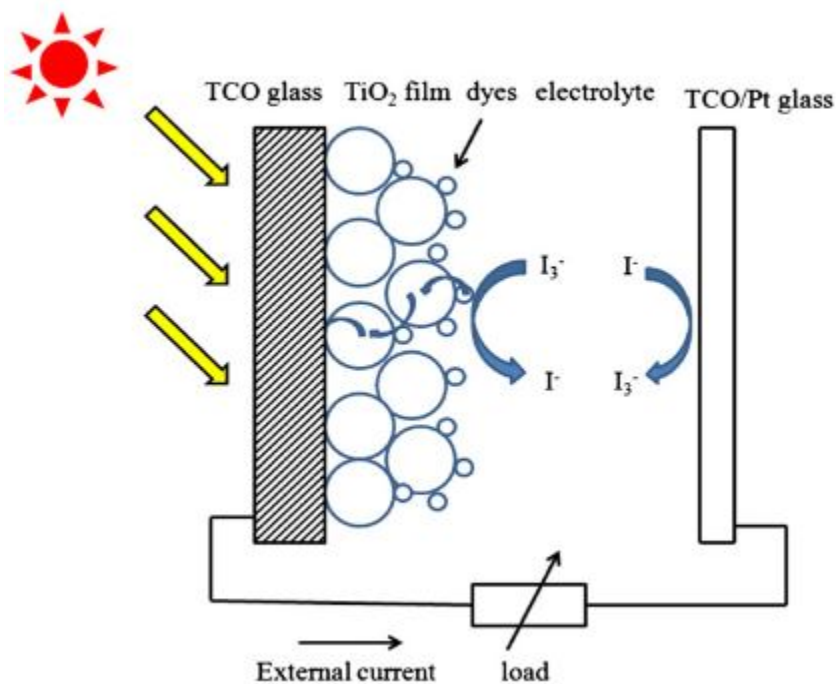
Fig 3.6 schematic diagram of dye-sensitize solar cell [8].

When exposed to sunlight, the dye sensitizer gets excited from which an electron is injected into the conduction band of the mesoporous oxide film. These generated electrons diffuse to the anode and are utilized at the external load before being collected by the electrolyte at cathode surface to complete the cycle. In order to enhance electrical conductivity and light transmittance, conducting glass is used as the substrate. There are mainly two types of conducting glass: indium-doped tin oxide (ITO) and fluorine-doped tin oxide (FTO). The standard to select a proper type is sometimes ambiguous because of the variety of cell configurations and materials. The semiconductor electrode is usually a layer of nano-crystalline titanium dioxide (TiO_2), a thin film deposited on the conducting glass film with the thickness 5–30μm, which plays an important role in both the exciton dissertation and the electron transfer process. The porosity and morphology of the TiO_2 layer are dominant factors that determine the amount of dye molecules absorbed on its surface which can provide an enormous area of reaction sites for the monolayer dye molecules to harvest incident light.

There are mainly two recombination mechanisms: the electrons recombine with the holes in the excited dye molecules; and the electrons reduce the triiodide to iodide ion. In fact, these two chemical reactions occur concurrently as competing reactions. Research has been done to compare their reaction kinetics with the photoelectron injection process. It was found that recombination between photo-injected electrons with oxidized dye molecules or I_3 ions occurs in microseconds $(10^6 s)$.Observed that the electron transfer dynamics betweenthe excited dye molecules into the TiO_2 conduction band is on the femtosecond $(10^{-15}s)$ scale by femtosecond mid-IR spectroscopy, whereas I ions reduce the oxidized dye on 10^{-8} seconds scale. Because the reduction rate of dye molecules is two orders of magnitude faster than the recombination with photoelectrons, the contribution of the former mechanism can usually be neglected. The dominant recombination reaction is represented by the reaction [8]:

$$I_3^- + 2e \rightarrow 3I^- \hspace{3cm} (3.2)$$

3.4.4 Solid-state dye-sensitized solar cells based on ordered ZnO nanowire arrays

A solid-state dye-sensitized solar cell (DSC) was fabricated by using arrays of 11-12 µm long, vertically oriented ZnO nanowire as the anode and CUSCN as the solid hole-transport material. The fabricated DSC yielded a power conversion efficiency of 1.7% under an irradiation of AM 1.5 sunlight [9].

3.4.5 Perovskite solar cell

In microelectronics, silicon has a combination of strengths that has made it difficult to displace as the favored photovoltaic material. Opportunities exist for technologies that promise either significantly higher energy conversion efficiencies or significantly lower processing costs. A new generation of mixed organic–inorganic halide perovskites offers tantalizing prospects on both fronts. Some key attributes of these perovskites include ease of fabrication, strong solar absorption and low non radiative carrier recombination rates for such simply prepared materials, plus the ability to capitalize on over 20 years of development of related dye-sensitized and organic photovoltaic cells. Perovskites are materials described by the formula ABX_3, where X is an anion and A and B are cations of different sizes (A being larger than B). The crystal structure of perovskites is depicted in Fig. a.

For the organic–inorganic halide perovskites of present interest, the larger cation A is organic; it is generally methylammonium (CH_3NH_3+) with R_A= 0.18 nm, although related ethylammonium ($CH_3CH_2NH_3+$) (R_A= 0.23 nm) and forma midinium ($NH_2CH=NH_2+$) (R_A is estimated to lie in the range 0.19–0.22 nm) also give good results. The anion X is a halogen, generally iodine (R_X= 0.220 nm), although Br and CL are also commonly used (R_X= 0.196 nm and 0.181 nm), usually in a mixed halide material. For efficient cells, cation B has universally been Pb(R_B= 0.119 nm); Sn (R_B= 0.110 nm) forms similar compounds with lower, theoretically more ideal bandgaps, but generally lower stability (attributed to the ease of oxidation of Sn to SnI_4 in the iodideperovskite; relativistic effects in the Pb counterpart are thought toprovide greater protection against oxidation). The archetypal compound is thus methylammonium lead triiodide ($CH_3NH_3PbI_3$), withmixed halides $CH_3NH_3PbI_{3-x}Cl_x$ and $CH_3NH_3PbI_{3-x}Br_x$ also beingimportant. Calculated and estimatedtandμfactors for a range ofthese perovskites are shown in Fig. 1b
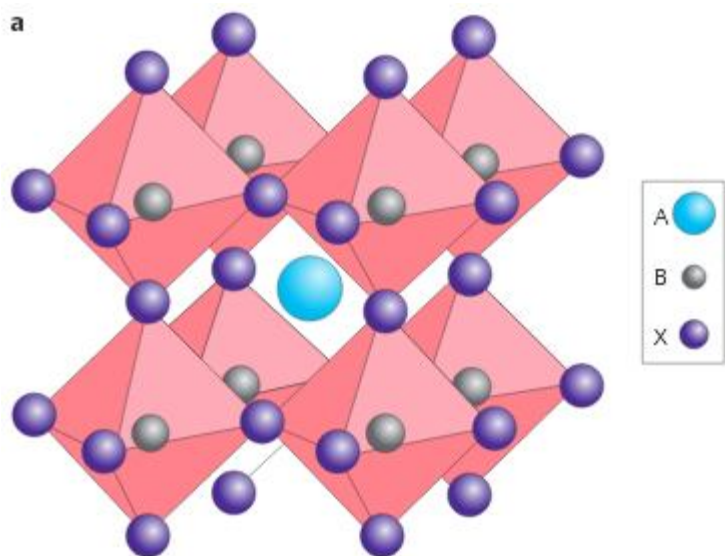

Fig 3.7 Perovskite crystal structure and associated tolerance and octahedral factors. A, Cubic perovskite crystal structure For photovoltaically interesting perovskites, the large cation A is usually the methylammoniumion(CH_3NH_3), the small cation B is Pb and the anion X is a halogen ion(usually I, but both CL and Br are also of interest) [10].

An organic electrolyte containing lithium halide and the corresponding halogen formed the hole-transporting medium (HTM), allowing positive contact. Attempts to replace this HTM with a solid-state HTM were not particularly successful [11]. Perovskite was shown to be deposited as sparsely spaced hemispherical nanoparticles that were approximately 2.5 nm in diameter. Perovskite nanoparticles exhibited better absorption than standard N719 dye sensitizers, but they dissolved in the electrolyte, resulting in a rapid degradation of performance. This stimulated the replacement of problematic electrolytes by a solid-state HTM. A spiroMeOTAD HTM was found to be effective in solid-state in dye cells. When dissolved in an organic solvent, spiro-MeOTAD penetrates nanoporous TiO_2, leaving only solute molecules after solvent evaporation. The cell structure is encompassed by the more general device of Fig 3.8, if the optional continuous perovskite layer is removed, leaving only scaffolding infiltrated by perovskite.

Almost simultaneously also success with spiro-MeOTAD along with four additional developments that split the field wide open. One of these developments was the use of the mixed-halide $CH_3NH_3PbI_{3-x}Cl_x$, which exhibited better stability and carrier transport than its pure iodide equivalent. A second involved going beyond earlier nanoparticle structures by coating nanoporous TiO_2 surfaces with a thin perovskite layer and thereby forming extremely thin absorber (ETA) cells. A third was replacing conducting nanoporous$TiO_2$by a similar but non-conducting Al_2O_3network. This improved the open-circuit voltage (V_{oc}); it also demonstrated that perovskites have a broader potential than just being used as sensitizers, as they are able to transport both electrons and holes between cell terminals. The fourth development exploited such ambipolar transport by demonstrating simple planar cells with the scaffolding Fig 3.8 completely eliminate. Both optional layers shown in Fig 3.8, including a solid perovskite capping layer overlying the scaffolding(nanoporous TiO_2 infiltrated by perovskite). Of the HTMs they investigated (which included spiro-MeOTAD), poly-triarylamine proved to be the best. Use TiO_2 scaffolding and two-step iodide deposition, which improved the morphology. The simpler structure allowed $CH_3NH_3PbI_{3-x}CL_x$ deposition by two-source thermal evaporation, again giving a better morphology. Both optional layers shown in Fig 3.8 were included, with the thickness ratio of perovskite-infiltrated TiO_2 scaffolding relative to the continuous perovskite layer being the key to the improved efficiency

Significantly, the latter three results were obtained using device structures that span all the possibilities inherent in Fig 3.8 left one or both optional layers, three different mixed-halide perovskites and two different HTMs were used.

Recent work has also demonstrated the use of new HTMs and electron transport media (ETMs). Effective ETMs which the standard fluorine-doped tin oxide (FTO)/compact TiO_2combination is replaced by indium tin oxide as a transparent conducting oxide combined with a thin (25 nm) ZnO-nanoparticle layer; gave high efficiency for planar cells on glass.

A
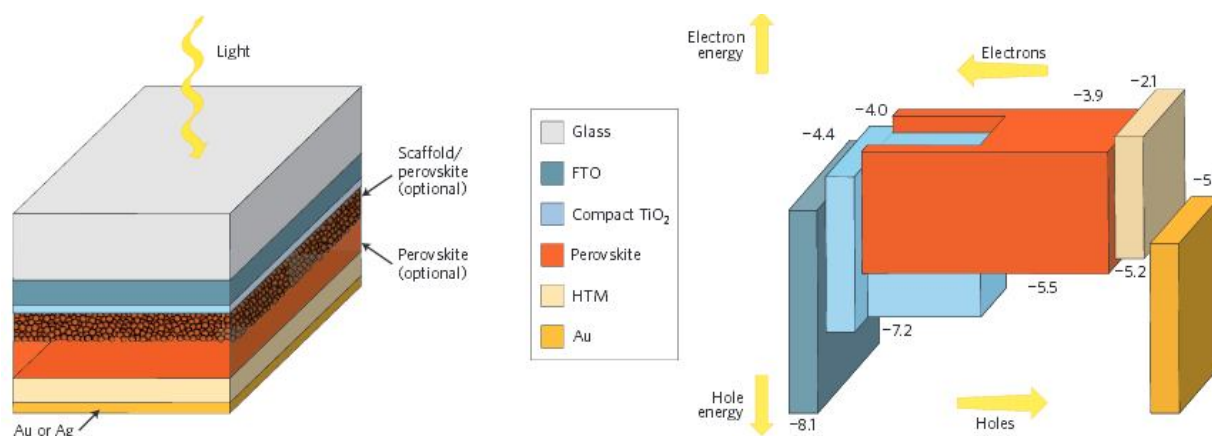
Fig3.8 Left**,**Perovskite cell structure and associated vacuum energy levels. A, General organic–inorganic halide solar cell, which includes two optional layers that are not essential for high performance; an energy conversion efficiency of over 15% has been reported for devices that have both optional layers, with only the scaffold layer infiltrated by the perovskite (and then by the HTM) and without scaffolding; the structure then corresponds to a simple planar thin film cell. Right, Vacuum energy levels (in eV) for corresponding materials (CH3NH3PbI3perovskite, conducting TiO2scaffold) [10].

3.4.6 Device engineering of perovskite solar cells to achieve near ideal efficiency
Theoretical calculations and detailed numerical simulations were used to provide the detailed balance limit efficiency in the presence of radiative and Auger recombination. Then, using coupled optical and carrier transport simulations, the physical mechanisms that contribute towards bias dependent carrier collection, and hence low fill factors of current perovskite based solar cells, were defined. The

simulations indicate that it is possible to achieve efficiencies and fill factors greater than 25% and 85%, respectively [11].

3.5 Electricity in Sudan

Presently, electricity generation is mainly by hydro (51%). The contribution of solar energy is not significant, Fig 3.10
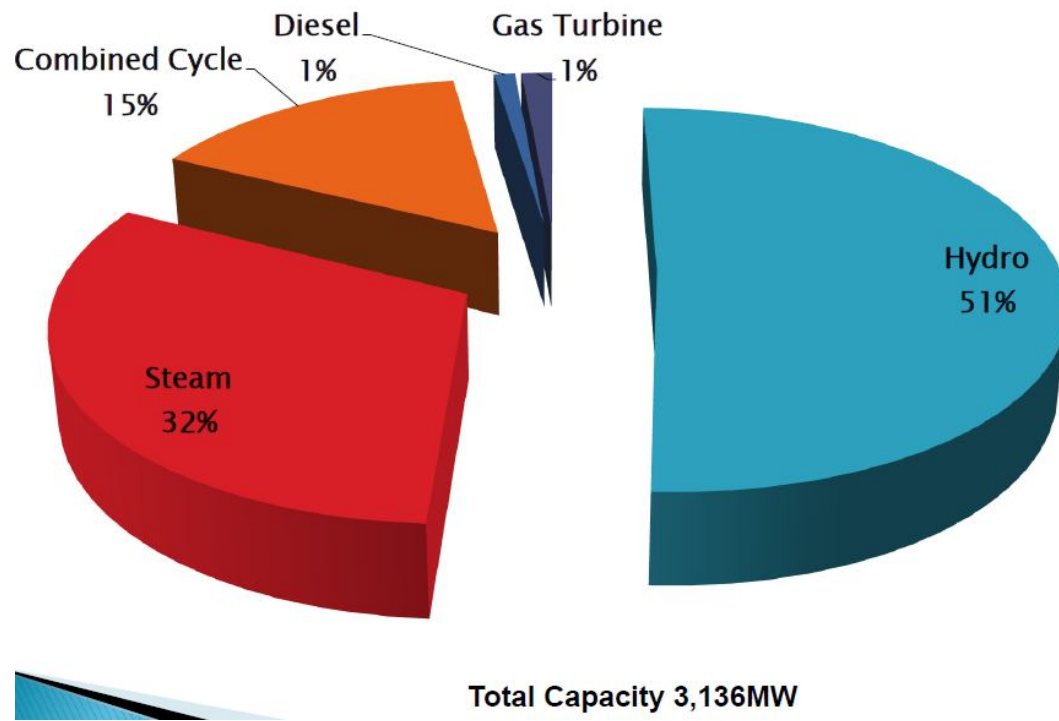
Fig 3.10 Electric generator in Sudan [2].

3.5.1 Solar energy current project

- 10 MW Khartoum Photovoltaic Power Plant
- 5 MW Nyala Photovoltaic Power Plant
- 3 MW Al Fashir Photovoltaic Power Plant
- 2 MW Al Geniena Photovoltaic Power Plant

3.5.2 Renewable energy – future plans

WRE prepared a Renewable Energy Master Plan (REMP) which aims to exploits the abundant renewable energy resources in Sudan. The following Fig 3.11 illustrates renewable energy master plan.
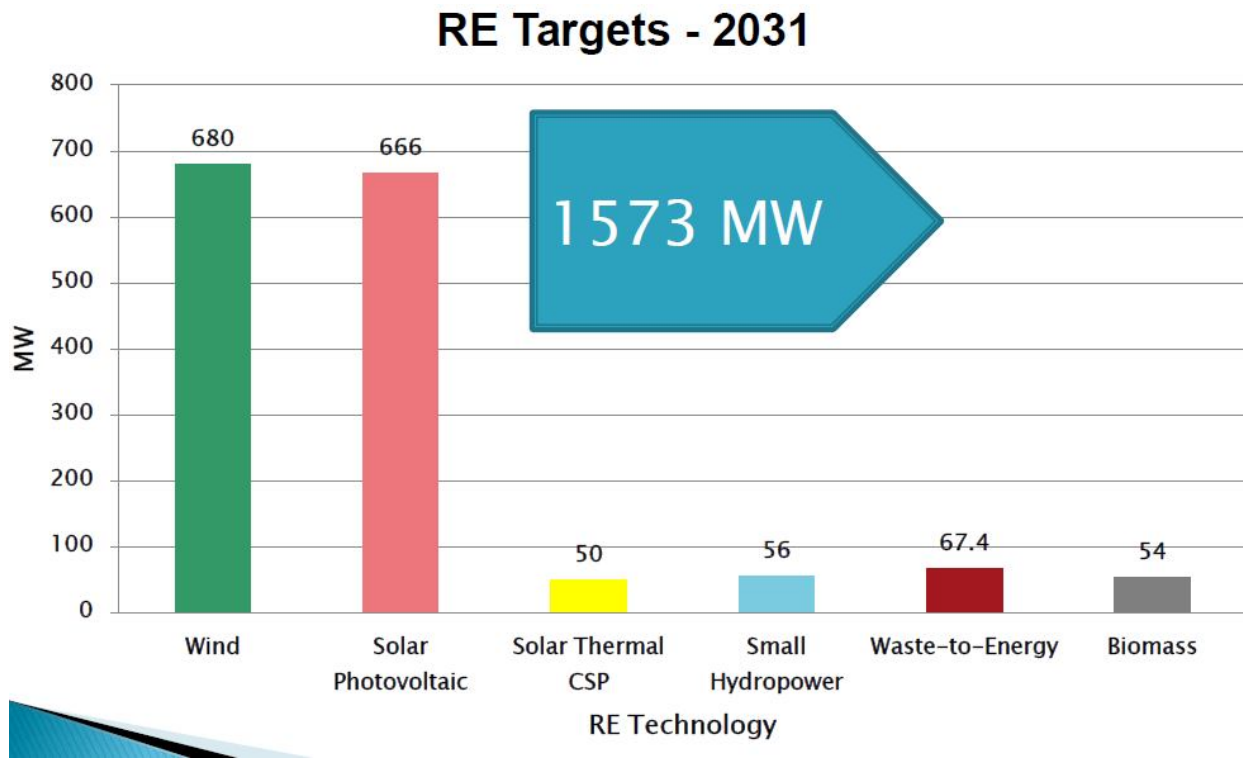
Fig 3.11 Renewable energy resource in Sudan.

In 2031: RE will represent 29.3% of the installed capacity13.6% share in the electricity generation [2].

In the Red Sea coast the solar radiation values are moderate, but the wind energy values are high. Both resources can be utilized in that area.

Chapter 4

Wind Atlas Analysis and Application Program (WAsP)

4.1 Introduction

In 1987 the Wind Energy and Atmospheric Physics Department at Risø National Laboratory introduced Wind Atlas Analysis and Application Program (WAsP) a powerful tool for wind data analysis, wind atlas generation, wind climate estimation, wind farm power production calculations and sitting of wind turbines. Over the years, the program has become the industry standard for wind resource assessment and sitting of wind turbines and wind farms [12].

4.2 WAsP PC-program

WAsP is a PC-program for the vertical and horizontal extrapolation of wind climate statistics. It contains several models to describe the wind flow over different terrains and close to sheltering obstacles. Conceptually, WAsP consists of five main calculation blocks:

4.2.1 Analysis of raw data

This option enables an analysis of any time-series of wind measurements to provide a statistical summary site-specific wind climate. This part is implemented in separate software tools: the Observed Wind Climate (OWC) Wizard and the WAsP Climate Analyst.

4.2.2 Generation of wind atlas data

Analyzed wind data can be converted into a regional wind climate or wind atlas data set. In a wind atlas data set the wind observations have been 'cleaned' with respect to site-specific conditions. The wind atlas data sets are site-independent and the wind distributions have been reduced to some standard conditions.

4.2.3 Wind climate estimation

Using a wind atlas data set calculated by WAsP or one obtained from another source the program can estimate the wind climate at any specific point by performing the inverse calculation as is used to generate a wind atlas. By introducing descriptions of the terrain around the predicted site, the models can predict the actual, expected wind climate at this site.

4.2.4 Estimation of wind power potential

The total energy content of the mean wind is calculated by WAsP. Furthermore, an estimate of the actual, annual mean energy production of a wind turbine can be obtained by providing WAsP with the power curve of the wind turbine in question.

4.2.5 Calculation of wind farm production

Given the thrust coefficient curve of the wind turbine and the Wind farm layout, WAsP can finally estimate the wake losses for each turbine in a farm and thereby the net annual energy production of each wind turbine and of the entire farm, i.e. the gross production minus the wake losses.

The program thus contains analysis and application parts, which may be summarized as follows:

4.3 Analysis

Time-series of wind speed and direction —> observed wind climate + meteorological station site description —> regional wind climate (wind atlas data sets)

4.4 Application

Regional wind climate + site description —> predicted wind climate.

Predicted wind climate + power curve —> annual energy production (AEP) of wind turbine

4.5 Wind farm production

Predicted wind climates + WTG characteristics —> gross annual energy production of wind farm

Predicted wind climates + WTG characteristics + wind farm layout —> wind farm wake losses

Gross annual energy productions + wake losses —> net annual energy production of wind farm

The WAsP models and the wind atlas methodology the figure to the right is a schematic presentation of the wind atlas methodology of WAsP [12].

4.6 Roughness

Estimation of the wind resource ranges from overall estimates of the mean energy content of the wind over a large area – called regional assessment – to the prediction of the average yearly energy production of a specific wind turbine at a specific location – called siting. The information necessary for siting generally needs to be much more detailed than in the case of regional assessment. However, both applications make use of the general concepts of topography analysis and regional wind climatology.

The collective effect of the terrain surface and obstacles, leading to an overall retardation of the wind near the ground, is referred to as the roughness of the terrain. However, not all the topographical elements contribute to the roughness. Vegetation and houses are examples of roughness elements, whereas long smooth hills, for example, are not, because they do not themselves cause an increase in the turbulence of the flow.

The terrain corresponding to roughness class 0 is water surface.

The terrain corresponding to different classes of roughness are:

(1) Class 0 is water surface.
(2) Class 1are open are with few windbreaks.
(3) Class 2 is farm land with wind-breaks.
(4) Class 3are urban districts, forests, and farm land with many windbreak

Chapter 5

Results and Discussion

5.1 Results

Wasp was used to analyze the wind data at three sites. The wind speed at different heights (10, 25, 50, 100, 200) and for different surface roughness (0, 1, 2, 3, 4) were obtained from the Wind Energy Project [12].The output from the program was mean wind speed and power density.

5.2 Tokar

The mean wind speed at different heights and different roughness are shown in table 5.1. At height 50 m, the mean wind speed is 8.33 m/s and mean power density is 584 W/m^2. Table 5.2 shows the wind climate at height 50 m. The highest wind speed frequency is 43.3% at speed 6.43 m/s and power density 229 W/m^2 in the northern direction.

Table 5.1 Wind speed and power density at Tokar.

		R-class0(0.000m)	R-class1(0.030m)	R-class2(0.100m)	R-class3(0.400m)
Height 1 (z=10m)	U[m/s]	7.10	5.06	4.39	3.44
	P[W/m^2]	375	147	95	46
Height 2 (z=25m)	U[m/s]	7.76	6.03	5.40	4.51
	P[W/m^2]	482	236	169	99
Height 3 (z=50m)	U[m/s]	8.33	6.93	6.30	5.43
	P[W/m^2]	584	334	253	164
Height 4 (z=100m)	U[m/s]	9.00	8.12	7.43	6.53
	P[W/m^2]	735	505	389	265

Table 5.2 Wind climate and power density at Tokar.

Sector		Wind climate		Power	Quality
Number	Angle[°]	Frequency[%]	Meanspeed[m/s]	Power density[w/m^2]	Speed discrepancy[%]
1	0	43.3	6.43	229	0.124 %
2	30	25.9	7.24	287	2.252 %
3	60	4.3	6.60	219	4.305 %
4	90	0.7	5.38	250	0.938 %
5	120	0.3	2.95	64	-1.703 %
6	150	0.3	2.38	14	3.216 %
7	180	0.8	4.34	139	-5.950 %
8	210	9.7	11.97	1322	2.776 %
9	240	3.1	6.79	338	0.713 %
10	270	1.9	4.82	141	-0.969 %
11	300	1.9	3.64	48	-1.034 %
12	330	7.8	5.17	124	1.517 %
All (emergent)			6.97	336	
Source data			6.88	335	

Wind direction is a significant element in wind energy analysis so that its knowledge would be really important to identify the optimum positioning for wind

turbine installations. On this account, the frequency for which the wind direction falls within different sectors should be identified. Fig 5.1illustrates the wind direction frequencies at the height of 50 m. Based on Fig. 5.1, it is observed that wind blows predominantly from North and North-East directions. The highest frequencies of wind directions are within 0° and 30°.
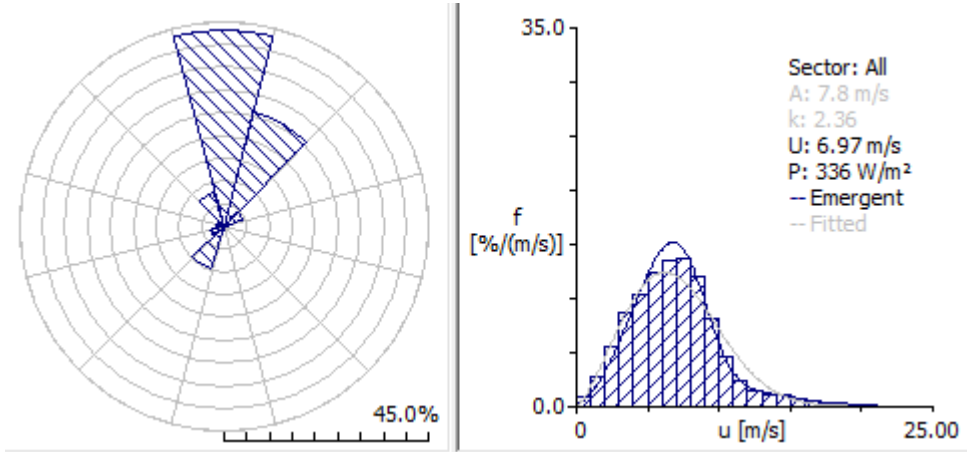

Fig 5.1 Windrose diagrams at 50 m height.

5.3 Free Zone

The mean wind speed at different heights and different roughness are shown in table 5.3. At height 50 m, the mean wind speed is 6.75 m/s and mean power density is 288 W/m^2. Table 5.4 shows the wind climate at height 50 m. The highest wind speed frequency is 31.8% at speed 6.05 m/s and power density 199 W/m^{2}in the northern direction.

Table 5.3 Wind speed and power density at Free Zone.

		R-class0(0.000m)	R-class1(0.030m)	R-class2(0.100m)	R-class3(0.400m)
Height 1 (z=10m)	U[m/s]	5.73	4.19	3.65	2.88
	P[W/m^2]	184	79	53	26
Height 2 (z=25m)	U[m/s]	6.28	5.01	4.51	3.79
	P[W/m^2]	236	127	93	56
Height 3 (z=50m)	U[m/s]	6.75	5.79	5.28	4.58
	P[W/m^2]	288	181	140	93
Height 4 (z=100m)	U[m/s]	7.31	6.83	6.27	5.54
	P[W/m^2]	372	285	220	151

Table 5.4 Wind climate and power density at Free Zone.

Sector		Wind climate		Power	Quality
number	Angle[°]	Frequency[%]	Meanspeed[m/s]	Power density[w/m²]	Speed discrepancy[%]
1	0	31.8	6.05	199	-0.885 %
2	30	21.6	6.92	257	2.393 %
3	60	11.2	5.99	159	1.689 %
4	90	4.6	5.19	107	3.539 %
5	120	1.9	4.28	90	2.708 %
6	150	1.0	3.61	69	-1.119 %
7	180	1.1	3.00	37	-1.800 %
8	210	1.3	3.10	51	-0.262 %
9	240	2.1	5.91	261	3.571 %
10	270	4.3	7.37	427	3.655 %
11	300	3.5	3.88	73	-3.195 %
12	330	15.5	5.73	157	1.187 %
All (emergent)			5.99	196	
Source data			5.93	195	

Fig 5.2illustrates the wind direction frequencies at the height of 50 m. Based on Fig 5.2, it is observed that wind blows predominantly from West directions. The highest frequencies of wind directions are obtained within 330˚ and 60˚.
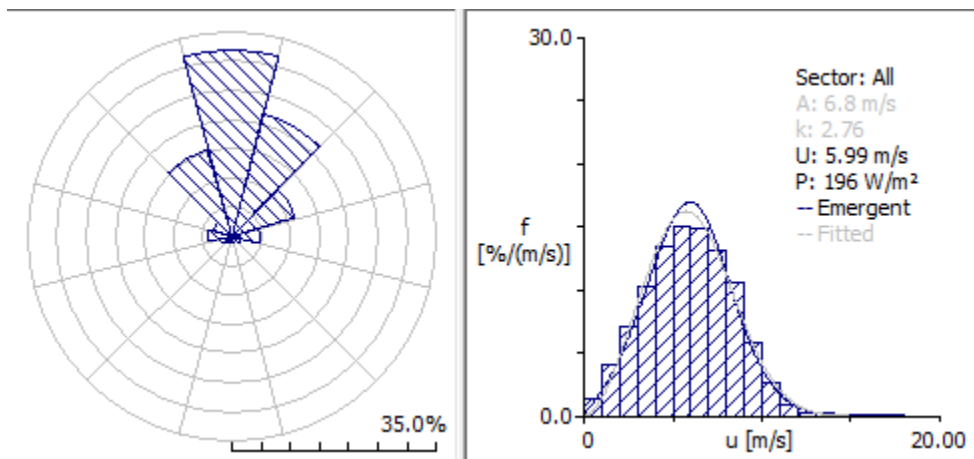
Fig 5.2 Windrose diagrams at 50m height.

5.4 Port Sudan

The mean wind speed at different heights and different roughness are shown in table 5.4. At height 50 m, the mean wind speed is 6.67 m/s and mean power density is 300 W/m^2. Table 5.6 shows the wind climate at height 50 m. The highest frequency is 30.8% at speed 6.01 m/s and power density 211 W/m^2 in the northern direction.

Table 5.5 Wind speed and power density at Port Sudan.

		R-class0(0.000m)	R-class1(0.030m)	R-class2(0.100m)	R-class3(0.400m)
Height 1 (z=10m)	U[m/s]	5.67	4.06	3.52	2.76
	P[W/m^2]	192	78	52	25
Height 2 (z=25m)	U[m/s]	6.21	4.86	4.34	3.63
	P[W/m^2]	246	126	91	54
Height 3 (z=50m)	U[m/s]	6.67	5.61	5.09	4.38
	P[W/m^2]	300	178	136	88
Height 4 (z=100m)	U[m/s]	7.23	6.63	6.05	5.30
	P[W/m^2]	389	280	214	143

Table 5.6 Wind climate and power densityat Port Sudan.

Sector		Wind climate		Power	Quality
number	Angle[°]	Frequency[%]	Meanspeed[m/s]	Power density[w/m²]	Speed discrepancy[%]
1	0	30.8	6.01	211	0.034 %
2	30	20.5	6.77	255	1.689 %
3	60	9.1	5.72	142	3.592 %
4	90	4.9	5.09	115	0.794 %
5	120	2.8	4.33	89	0.298 %
6	150	1.8	2.93	42	-4.436 %
7	180	1.3	2.80	27	-1.481 %
8	210	1.7	2.82	27	-0.421 %
9	240	1.3	2.66	31	-2.367 %
10	270	3.3	6.19	343	3.027 %
11	300	3.7	3.36	50	-0.771 %
12	330	18.7	5.39	132	1.965 %
All (emergent)			5.64	178	
Source data			n/a	n/a	

Fig 5.3illustrates the wind direction frequencies at the height of 50 m. Based on Fig 5.3, it is observed that wind blows predominantly from North-East directions. The highest frequencies of wind directions are within 330° and 60°.
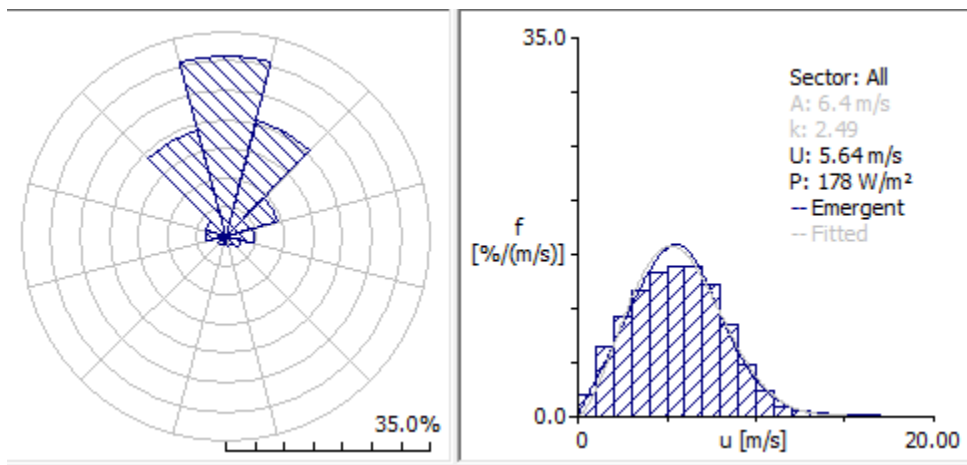

Fig 5.3 Windrose diagrams at 50 m height.

Chapter 6

Conclusion and Recommendation

6.1 Conclusion

Both wind and solar energy are available in the Red Sea coast. The mean wind power density at 80 m height is about 8 kWh m^{-2}/day, while the mean solar power density is about 5kWh m^{-2}/day.

WAsP was used to calculate the mean wind speed and mean wind power density at the three sites. At 50 m height, the wind power density at Tokar, free zone and north Port Sudan were 584, 288 and 300 W/m^2, respectively. In all sites the direction of the wind is from the north.

There is high wind power density and moderate values of solar radiation at the Red Sea coast. The most suitable renewable energy system for the Red Sea coast could be a hybrid system consisting of wind turbines with the backup of a photovoltaic system.

6.2 Recommendations

It is recommended that a prototype, cost-effective hybrid system is to be designed for the Red Sea coast. The system is to consist of wind turbines and photovoltaic system. It must be design with minimum storage system. Storage system is to cover the difference between the supply and demand of electricity during night time.

References

[1] C. Dan. Wind Power Basics, New Society Publishers, New York, 2010.

[2] Ministry of Water Resources and Electricity, Sudan, 2015.

[3] Y. Kumar, etal, Wind energy: Trends and enabling technologies, Renewable and Sustainable Energy Reviews 53, 2016.

[4] M. Ritter, etal, Designing an index for assessing wind energy potential, Renewable Energy 83, 2015.

[5] B. Van Zeghbroeck, Principles of Semiconductor Devices, - www.colorado.edu/~bart/book, 2002.

[6] R. Kapadia, et al, Nanopillar photovoltaics: Materials, processes, and devices, Nano Energy 1, 2012.

[7] H. Yang, etal, Organic solar cells employing electrodeposited nickel oxide nanostructuresas the anode buffer layer, Solar Energy Materials & Solar Cells, 101, 2012.

[8] J. Gong, et al,Review on dye-sensitized solar cells (DSSCs): Fundamental concepts andnovel materials, Renewable and Sustainable Energy Reviews,16, 2012.

[9]U. V Desai, etal, Solid-state dye-sensitized solar cells basedon ordered ZnO nanowire arrays, Nanotechnology, 23, 2012.

[10]M. A. Green, etal, The emergence of perovskite solar cells, nature photonics, 134, 2014.

[11]S. Agarwal, etal,Device engineering of perovskite solar cells to achieve near ideal efficiency, Applied Physics Letters,107, 2015.

[12] Wind Energy Project, UNDP, Khartoum, 2016.